



High temperature oxidation of CoAl(100)

Volker Rose^{*}, Vitali Podgursky, Ioan Costina, René Franchy[✱], Harald Ibach

Institut für Schichten und Grenzflächen (ISG 3) des Forschungszentrums Jülich, D-52425 Jülich, Germany

Received 29 September 2004; accepted for publication 22 December 2004

Available online 19 January 2005

Abstract

We have employed Auger electron spectroscopy (AES), high resolution electron energy loss spectroscopy (EELS), low energy electron diffraction (LEED) and scanning tunneling microscopy (STM) to investigate the growth of an Al₂O₃ film on CoAl(100). While exposure to oxygen at room temperature leads to the formation of amorphous alumina, subsequent annealing at higher temperatures results in the growth of well-ordered θ -Al₂O₃. Well-ordered Al₂O₃ films are also formed by oxidation at temperatures of 800 K and above. The oxide is characterized by Fuchs–Kliwer modes at around 430, 630, 780 and 920 cm⁻¹. Oxide islands grow in two sets of domains perpendicular to each other. Under ultra-high vacuum conditions, self-limiting thickness of the oxide layer (9–10 Å) has been found. The band gap of the θ -Al₂O₃ film on CoAl(100) is 4.3–4.5 eV.

© 2005 Elsevier B.V. All rights reserved.

Keywords: AES; LEED; EELS; STM; Oxidation; Cobalt; Aluminum; Alumina

1. Introduction

The metal oxide interface is of considerable intrinsic interest. Also it is of extreme importance in many technological applications including heterogeneous catalysis [1] or magnetoelectronic devices [2]. In particular, well-ordered oxide

surfaces play a key role in the understanding of metal oxide interfaces. In the last years the oxidation of low index intermetallic alloy surfaces, such as NiAl, Ni₃Al, CoGa [3], or FeAl [4], has been intensively studied. Generally, the authors report about the growth of well-ordered Al₂O₃ films at high oxidation temperatures. Due to thermodynamic reasons the oxidation of this intermetallic alloys is restricted to the Al atoms, while the Ni, Co and Fe atoms remain unaffected. Furthermore, it has been shown that different transient modifications of thin alumina films can be fabricated at varying oxidation temperatures. CoAl is an

^{*} Corresponding author. Present address: Argonne National Laboratory, Argonne, IL 60439, USA. Tel.: +49 2461 61 5765; fax: +49 2461 61 3907.

E-mail address: v.rose@fz-juelich.de (V. Rose).

[✱] Deceased.

intermetallic alloy with CsCl-type structure (B2) with a lattice constant of 2.862 Å [5]. The (100) layers have an ABAB... stacking sequence. The melting point is 1913 K. The clean CoAl(100) surface shows a (1 × 1) LEED pattern with sharp Bragg reflections [6]. The surface is terminated by a nominal Al sublattice with approximately 30% of Co atoms therein caused by antisite atom segregation [7], and exhibits 400–1000 Å wide terraces separated by double atomic steps.

Our previous work [6] has shown that oxygen exposure of CoAl(100) at room temperature leads to the formation of amorphous alumina (a-Al₂O₃). After saturation with oxygen the thickness of the a-Al₂O₃ film was estimated to be around 7 Å. Wide energy range electron energy loss spectroscopy (EELS) measurements showed that the band gap of this oxide is 3.2 eV.

The main purpose of this paper is the presentation of the oxidation of CoAl(100) in a wide temperature range and to discuss the formation of well-ordered alumina films. For that reason the oxidation of CoAl(100) is studied by Auger electron spectroscopy (AES), high resolution electron energy loss spectroscopy (EELS), low energy electron diffraction (LEED) and scanning tunneling microscopy (STM).

2. Experimental

The experiments were carried out in an ultra high vacuum (UHV) system with a base pressure typically of 8×10^{-11} mbar. The chamber was equipped with a cylindrical mirror analyzer (CMA) for AES, an EEL spectrometer [8], a three-grid LEED optics and a STM microscope. A quadrupole mass spectrometer (QMS) was used for the residual gas analysis. The surface sensitivity of AES was improved by decreasing the incidence angle (3°) of the electron gun in addition to a normal incidence using the same CMA. The EEL spectra were taken in specular geometry at an incident angle of 57° with respect to the normal of the CoAl(100) surface and at primary energies of around 4 eV for vibrational studies and 16 eV for wide energy scans required to determine the band gap. The STM microscope was a modified version

of the Beetle type developed by Besocke [9] and was operated in a constant current mode. The sample was annealed by electron bombardment. Temperature was measured by a WRe25%–WRe3% thermocouple mounted directly to the back of the sample. During the adsorption steps the oxygen partial pressure was adjusted between 1×10^{-6} and 1×10^{-8} mbar. The exposure is given in L units (1 L = 1.3×10^{-6} mbar s). During our investigations presented in Section 3.2, oxidation took place at room temperature and the sample was subsequently annealed for 2 min at each step.

Our CoAl(100) substrate crystal had a diameter of 10 mm and a thickness of 2.1 mm. The accuracy of orientation was 0.1° after mechanical polishing.

The surface of the substrate was cleaned in UHV by several cycles of Ar⁺ ion sputtering (2 μA, 1 kV, 20 min) and by subsequent annealing at 1470 K (10 min). Residual carbon contamination was removed by several cycles of heating to 1200 K in an O₂ atmosphere at 1×10^{-6} mbar for 2 min followed by 2 min of annealing at 1470 K.

3. Results and discussion

3.1. The clean CoAl(100) surface

The dotted line in Fig. 1a represents the low energy region of an AES spectrum of the clean CoAl(100) surface measured with an electron gun in normal incidence geometry (NIAES). The spectrum exhibits the transitions of Co (MNN at 53 and 95 eV) and Al (LMM at 68 eV). The same transitions occur when the primary electrons hit the surface under grazing incidence (GIAES) conditions (Fig. 1b). A detailed analysis and comparison of AES spectra for both geometries allows a conclusion about the termination of the surface. The peak-to-peak ratio $CO_{MNN}(53 \text{ eV})/Al_{LMM}(68 \text{ eV})$ amounts to 1.1 in NIAES, whereas in GIAES this ratio decreases to 0.9. The latter measurements prove that the Co/Al ratio varies within the top atomic layers, e.g. the layers are enriched with Al atoms. This corroborates our earlier investigations [6] and has been explained by antisite atom segregation of Co atoms to the nominal Al sublattice in the topmost surface plane [7].

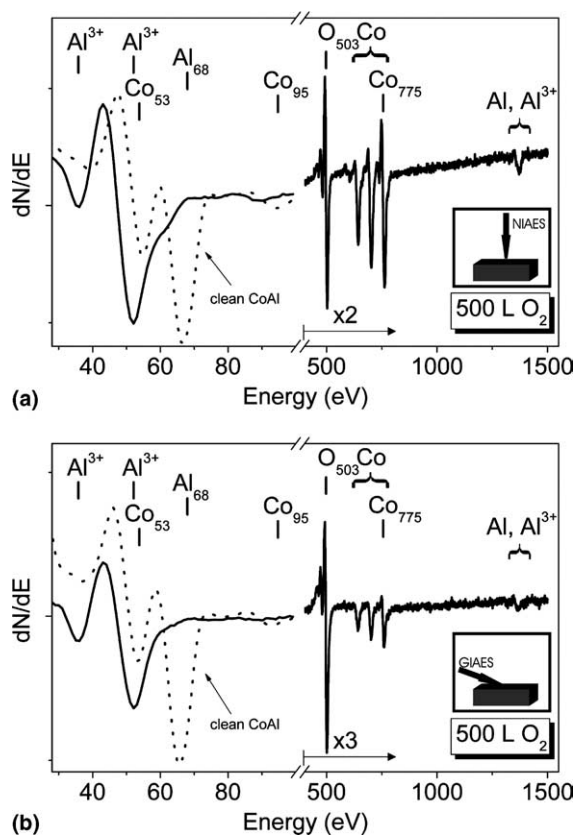


Fig. 1. AES spectra of the oxidation of CoAl(100) at 800 K (a) investigated with a normal incidence primary electron gun (NIAES) and (b) in grazing incidence conditions (GIAES). The dotted line shows the low energy region of AES spectra obtained for clean CoAl(100).

3.2. Oxidation of CoAl(100) at 800 K

Fig. 1a shows an NIAES spectrum after the oxidation of CoAl(100) with 500 L of O₂ at 800 K. In addition to the characteristic transitions of the clean sample, i.e. Co (MNN at 53 and 95 eV, LMM at 656, 716 and 775 eV) and Al (LMM at 68 and 84 eV, KLL at 1396), the transitions of O (KLL at 503) and Al³⁺ (MNN at 35 and 53 eV, KLL at 1378 eV) are observed. The Co_{MNN} (53 eV) peak overlaps with the Al³⁺ (51 eV). The transition at around 1383 eV is generated by the overlap of Al_{KLL} (1396 eV) and Al³⁺ (1378 eV). It appears that an alumina layer is formed on the surface. The formation of Al₂O₃ is facilitated by the fact that the heat of alumina formation

($\Delta H_f = -1675 \text{ kJ mol}^{-1}$) is about twice the value necessary for Co₃O₄ formation (-891 kJ mol^{-1}) and about seven times the value needed to form CoO (-238 kJ mol^{-1}) [10]. GIAES conditions (Fig. 1b) yield a spectrum for 500 L of O₂ on CoAl(100) with nearly the same transitions but with different relative intensities. The intensity of Co LMM transitions decreases substantially with respect to the O_{KLL} (503 eV) peak. While the ratio of Co_{LMM} (775 eV)/O_{KLL} (503 eV) amounts to 0.70 for NIAES, a decrease to 0.15 can be found for GIAES. In addition, the Al_{LMM} (68 eV) transition appears only as a weak shoulder. This is a consequence of the improved surface sensitivity of GIAES, e.g. screening of the CoAl transitions through the oxide layer. The KLL transitions of Al and Al³⁺ are not resolved and produce a peak at around 1376 eV. This shift of 7 eV in comparison to the NIAES measurement indicates the strengthened influence of Al³⁺ in the near surface region.

Fig. 2 shows the peak-to-peak ratio of the NIAES transitions of O_{KLL} (503 eV) and Co_{LMM} (775 eV) as a function of O₂ exposure. The intensity of the O_{KLL} (503 eV) transition is normalized to the intensity of the oxygen-saturated surface, whereas the intensity of the Co_{LMM} (775 eV) transition is normalized to the intensity of the clean CoAl surface. The curves reveal a high initial sticking probability up to an exposure of around 30 L.

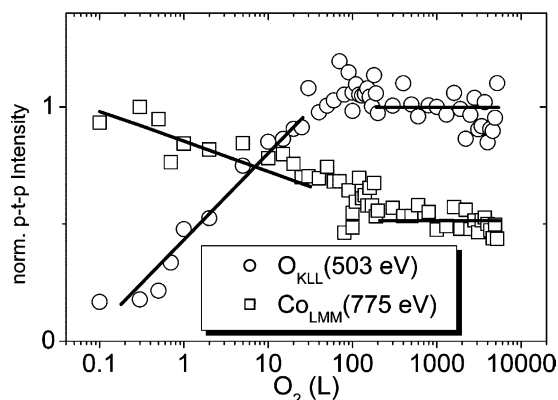


Fig. 2. Normalized peak-to-peak intensity of O_{KLL} (503 eV) and Co_{LMM} (775 eV) NIAES transitions as a function of O₂ exposure.

Already after 1.5 L O₂ the intensity of the O_{KLL} (503 eV) transition reaches half of its saturation value. For exposures above 200 L, the O₂-uptake levels off, suggesting that the surface oxidation is complete. The intensity of the Co_{LMM} (775 eV) transition decreases to 83% of its initial value after 1.5 L O₂, and the signal intensity saturation at $I = 0.52$ can be found for exposures above 200 L O₂. A logarithmic growth-rate of Al₂O₃ and saturation for high oxygen doses was also reported for the NiAl and Ni₃Al surfaces (see Table 1) and can be explained by the theory of Cabrera and Mott [11]. After reaching a certain thickness the electric field between the O²⁻ and the metal ions driving the growth of the oxide, is insufficient to account for ion movement. The attenuation of the Co intensity is a consequence of the substrate signal screening due to the growth of alumina on top of the surface. We can estimate the oxide thickness t of the overlayer using the equation

$$t = -\lambda \cdot \cos \omega \cdot \ln(I)$$

where $\lambda = 18 \text{ \AA}$ is the inelastic mean free path for 775 eV electrons in alumina [12]. The entrance angle of the CMA is $\omega = 42^\circ$. Hence, the thickness of the oxide film after the saturation is estimated to be 8.8 Å and exceeds the thickness of the amorphous Al₂O₃ film grown on CoAl(100) at room temperature [6].

The EEL spectra for different oxygen exposures at 800 K are shown in Fig. 3. After the exposure of 0.2 L of O₂ the spectrum shows four phonons at 235, 430, 635 and 880 cm⁻¹. The mode at 235 cm⁻¹ can be assigned to a quasi-transverse optical

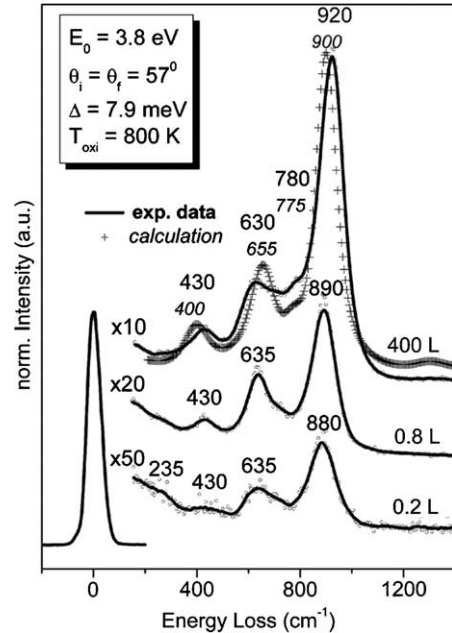


Fig. 3. Set of EEL spectra of the growth of Al₂O₃ on CoAl(100). In order to distinguish the different spectra, they are vertically shifted. A calculated EEL spectrum is marked by plus signs.

mode arising from the perpendicular vibration of Al atoms at the oxide/substrate interface. A similar loss was already observed on NiAl(110) [13] and NiAl(111) [13,14] surfaces. After the exposure of 0.8 L of O₂ this loss vanishes because the oxide coverage becomes sufficient to screen the Al vibration. The remaining losses gain intensity, and the mode initial 880 cm⁻¹ shifts slightly to 890 cm⁻¹.

Table 1

The characteristic frequencies of the losses in the EEL spectra and the band gap for well-ordered Al₂O₃ films on surfaces of different intermetallic alloys

Well-ordered Al ₂ O ₃ on	FK modes (cm ⁻¹)	Oxidation temperature (K)	Structure	Bandgap (eV)	References
NiAl(100)	400, 600, 900	700–1200	γ'-Al ₂ O ₃		[17]
	420, 603, 718, 896	1200	θ-Al ₂ O ₃		[17]
NiAl(110)	410, 620, 850	1200	γ'-Al ₂ O ₃		[18]
NiAl(111)	427, 637, 887	900–1100	γ'-Al ₂ O ₃		[19]
	629, 911	>1100	α-Al ₂ O ₃		[19]
Ni ₃ Al(100)	415, 640, 875	1150	γ'-Al ₂ O ₃	4.3	[20]
Ni ₃ Al(111)	440, 648, 910	1000	γ'-Al ₂ O ₃		[21]
Al(111)	~435, ~665, 887	500			[22]
CoAl(100)	430, 630, 780, 920	800	θ-Al ₂ O ₃	4.5	This work

With further increasing exposure, both the shift of this mode and the gain of intensity of all modes continue. The EEL spectrum of 400 L O₂ exhibits modes at 430, 630 and 920 cm⁻¹ and a weak phonon at 780 cm⁻¹. The loss structure is attributed to the Fuchs–Kliwer (FK) modes [15,16] of a well-ordered alumina layer. The rather large losses are indicative of an oxide overlayer and caused by the strong metal-oxide dipoles. Our results are in good agreement with the investigations of the growth of different phases of well-ordered alumina films on NiAl(100) [17], NiAl(110) [18], NiAl(111) [19], Ni₃Al(100) [20], Ni₃Al(111) [21], or Al(111) [22] (see Table 1). Generally, all aluminium oxides consist of a close-packed oxygen sub-lattice with Al cations assuming the positions of the tetrahedral and/or octahedral vacancies. Different occupation probabilities of the vacancies determine the crystal structure. According to group theory four IR active modes are expected for γ -like or θ -like phases (Al ions in tetrahedral and octahedral vacancies) whereas in hexagonal α -Al₂O₃ the octahedral sites are solely occupied and only two FK modes can be obtained [19]. The EEL spectra of the γ -like or θ -like phases like here commonly show three distinct phonon features in the frequency region of 400–440 cm⁻¹, 600–648 cm⁻¹ and 850–910 cm⁻¹ whereof a fourth loss remains normally unresolved due to the broadness of the loss structure. However, in the

case of θ -alumina on NiAl(100) in addition a fourth loss at 718 cm⁻¹ was reported [17].

The comparison between measured and calculated EEL spectra based on dielectric theory can give important indications about structure and thickness of oxide films. We employed a program published by Lambin et al. [23] to simulate EEL spectra for electrons specularly reflected from the surface. Because of missing data for CoAl, parameters taken from NiAl [24] alloy were used. Table 2 lists the IR parameters [25] we used to simulate a γ -Al₂O₃ film on NiAl. A calculated spectrum is presented in Fig. 3 (marked by plus signs). Calculations show that variation of the oxide thickness leads to small energy shifts of the FK modes (<50 cm⁻¹) while the number and the relative intensities of the peaks remain constant. Best agreement between measurement and calculation is found for oxide thickness of 10 Å at which FK modes at 400, 655, 775 and 900 cm⁻¹ occur, in agreement with the thickness obtained from AES analysis. The loss at 1300 cm⁻¹ can be assigned to a multiple excitation. Although EEL spectra can ensure that the alumina film is well-ordered, further determination of the oxide structure can only be carried out with LEED experiments.

Fig. 4 shows LEED patterns of the CoAl(100) surface after oxidation at 800 K with 0.7 and 100 L O₂. After the exposition with 0.7 L oxygen

Table 2

Oscillator parameters that were used for the calculated EEL spectrum in Fig. 3 of a θ -Al₂O₃ film with a thickness of 10 Å (for elucidations of the variables see [23])

γ -Al ₂ O ₃							
Dielectric constant		Thickness of the layer = 10 Å					
ϵ_0	2.9	Thick	.10D + 02				
Resonant frequency (cm ⁻¹)	Strength factor		Resonant frequency (cm ⁻¹)		Damping constant		
ω_{TO1}	357.0	S_{k1}	2.52	ω_{LO1}	403.0	γ_k/ω_{TO1}	0.202
ω_{TO2}	536.0	S_{k2}	2.38	ω_{LO2}	669.0	γ_k/ω_{TO2}	0.189
ω_{TO3}	744.0	S_{k3}	0.34	ω_{LO3}	783.0	γ_k/ω_{TO3}	0.076
ω_{TO4}	807.0	S_{k4}	0.17	ω_{LO4}	917.0	γ_k/ω_{TO4}	0.054
Substrate (NiAl)							
Bulk plasmon frequency (eV)	Thickness is assumed infinity			Damping frequency			
ω_p	7.4	Thick	.100D + 75		γ	0.03	

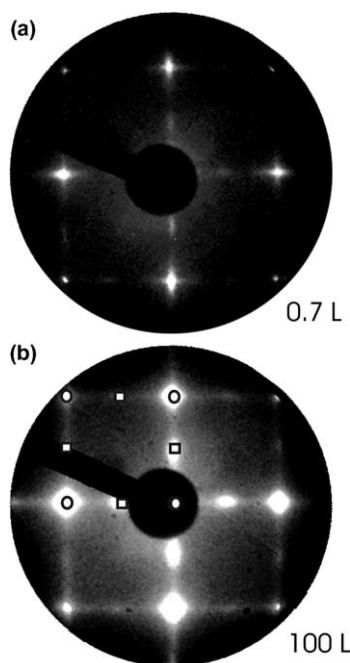


Fig. 4. The LEED images of (a) 0.7 and (b) 100 L of O_2 on CoAl(100) exhibit a (2×1) structure with weak streaks ($E_p = 75$ eV). Some reflexes are marked for better understanding.

(Fig. 4a) LEED shows (1×1) pattern of the clean surface [6], a two-domain (2×1) structure, as well as weak streaks along the $[100]$, and the $[010]$ directions. With increasing oxygen dosage the spots and streaks gain intensity. For the sake of clarity the spots of one unit cell have been marked in Fig. 4b. Based on the LEED measurements, e.g. appearance of a (2×1) pattern, we conclude that a well-ordered θ - Al_2O_3 film grows on CoAl(100).

The presence of streaks in LEED patterns is usually assigned to a loss of order in the corresponding direction. Such streak structures are also reported for the high temperature oxidation of FeAl [4]. For Al_2O_3 on NiAl(100) high-resolution spot profile analysis of low energy electron diffraction (SPALED) exhibits a satellite structure in the pattern corresponding to a (9×1) superstructure [26]. It was found that the crystalline Al_2O_3 strips are embedded in re-grown NiAl terraces ($c(\sqrt{2} \times 3\sqrt{2})R45^\circ$) and areas of ultra-thin layers

of α - Al_2O_3 . This suggests a complicated interface structure favouring the formation of Al_2O_3 stripes. In a surface X-ray diffraction study [27] on the oxidation of the NiAl(100) it was found that the islands of θ - Al_2O_3 are embedded in a matrix of alumina layers showing a strong deviation from the pure θ -phase at the metal-oxide interface and at the oxide surface. Thus, the growth of a perfectly ordered, pure θ - Al_2O_3 layer on NiAl(100) producing a streak-free (2×1) structure is somewhat complicated. We believe the scenario described above for NiAl(100) may be also valid for the oxidation of CoAl(100).

Fig. 5a shows a STM image of CoAl(100) taken after the oxidation with 10 L of oxygen. Rectangular domains rotated 90° with respect to each other can be observed containing a unit cell with the lengths of the basis vectors $a \sim 2.9$ Å and $b \sim 5.7$ Å. Such unit cell corresponds to the θ - Al_2O_3 layer and explains the (2×1) structure observed by LEED. A top view structure model of the oxide is depicted in Fig. 5b. In each oxygen layer of θ - Al_2O_3 the Al ions form chains with a distance of $b = 5.64$ Å. Thus the stripes in the STM image can be either connected to aluminium chains or Al missing chains. In case of the β - Ga_2O_3 , that is isomorphic to θ - Al_2O_3 , comparable stripes were explained by Ga-missing rows with a depletion of charge of Ga due to electron transfer to O during oxidation [28]. Because we have used a positive bias voltage at the tip a charge transfer from Al to O in θ - Al_2O_3 favours the interpretation of Al missing chains.

Fig. 5c shows a qualitative 3D structural model of a θ - Al_2O_3 thin film on CoAl(100). The θ - Al_2O_3 phase exhibits a monoclinic unit cell ($a = 2.92$ Å, $b = 5.64$ Å, $c = 11.78$ Å, $\beta = 104^\circ$). Depending on the domain orientation, the (110) plane of the fcc oxygen sublattice is parallel to the $[100]$ or $[010]$ direction of CoAl. Further, the oxygen (110) plane is perpendicular to the CoAl(100) surface. This is the classical Bain orientation between bcc CoAl and the fcc oxygen sublattice structure. According to this, the lattice mismatch between CoAl(100) and θ - Al_2O_3 only amounts to $\sim 1\%$ in a -axis direction ($a_{\theta\text{-alumina}} = 5.64$ Å, $2 \times a_{\text{CoAl}} = 5.72$) and $\sim 2\%$ in the b -axis direction ($b_{\theta\text{-alumina}} = 2.91$ Å, $b_{\text{CoAl}} = 2.86$ Å). Therefore,

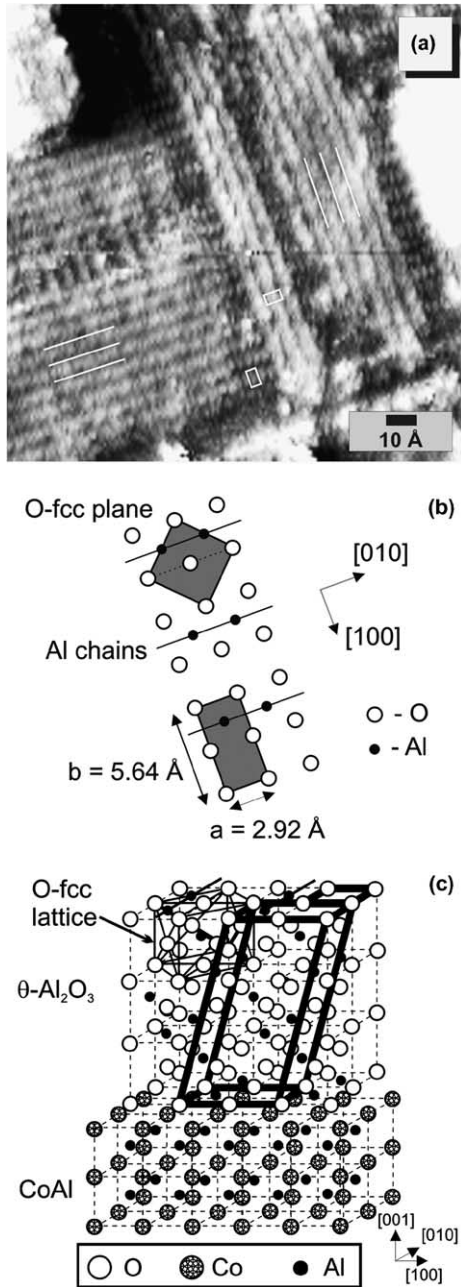


Fig. 5. (a) STM image of 10 L O_2 on CoAl(100) at 800 K ($U_t = 2.00$ V, $I_t = 0.2$ nA). The two domains of the oxide film are denoted by the white stripes. For each domain a unit cell is outlined. (b) Top view model of the θ - Al_2O_3 surface plane. (c) The structure model of θ - Al_2O_3 grown on CoAl(100). In addition a monoclinic θ - Al_2O_3 unit cell and the close-packed oxygen fcc lattice is marked. For the sake of clarity, only the octahedral occupation of Al^{3+} ions is shown.

the θ - Al_2O_3 is compressed in one direction and expanded in the perpendicular direction.

Fig. 6a–d show wide area STM images of CoAl(100) at different stages of oxidation. Due to experimental reasons we had to remove the STM from the sample during the oxidation steps. However, while every image corresponds to a different area of the sample surface it demonstrates a surface morphology typical to the particular oxidation step. The clean surface (Fig. 6a) exhibits 12 large terraces with a width of around 400–1000 Å separated by 2.8 Å steps with assigned to double atomic steps of the CsCl structure of CoAl [6]. Already after the exposure to 0.5 L of oxygen the number of terraces decreases to 8 and a rearrangement of the steps can be recognized. Only rectangular angles are found on the steps between two terraces. The step heights amount to ~ 3 Å which shows that the oxidation takes place on top of all terraces in the same way. In addition, on top of the terraces elongated Al (missing) chains can develop, starting from the step edges in directions perpendicular to each other (see arrows). After the exposure of 1 L O_2 (Fig. 6c) the oxide islands preferentially start from the step edges (white arrows). In addition, two types of isolated islands (Is_a and Is_b) with rectangular shape appear growing parallel to the step edges. Isolated islands like marked as Is_a appear as trenches on the CoAl surface (such as the oxide located at the steps) and the Is_b islands show up as protrusions on the same terraces. Thus, the lateral growth of the oxide is accompanied by a height growth with the formation of oxygen islands of a distinct height. After the sample exposure to 100 L of O_2 (Fig. 6d) the surface is entirely covered with oxide. The oxide domains and the chain structure are very well visible over the whole surface. The nanostructured Al_2O_3 exhibits stripes indicated by arrows that are oriented in the domain directions starting at the step edges featuring length up to several hundred Å. The discrete distribution of the stripe width (Fig. 7) exhibits a pronounced maximum at 68 Å and a secondary maximum around 135 Å. These values are multiples (12 times and 24 times respectively) of the lattice constant $b = 5.64$ Å of θ - Al_2O_3 . The latter observation may result from a periodical change of the accumulated energy perpendicular

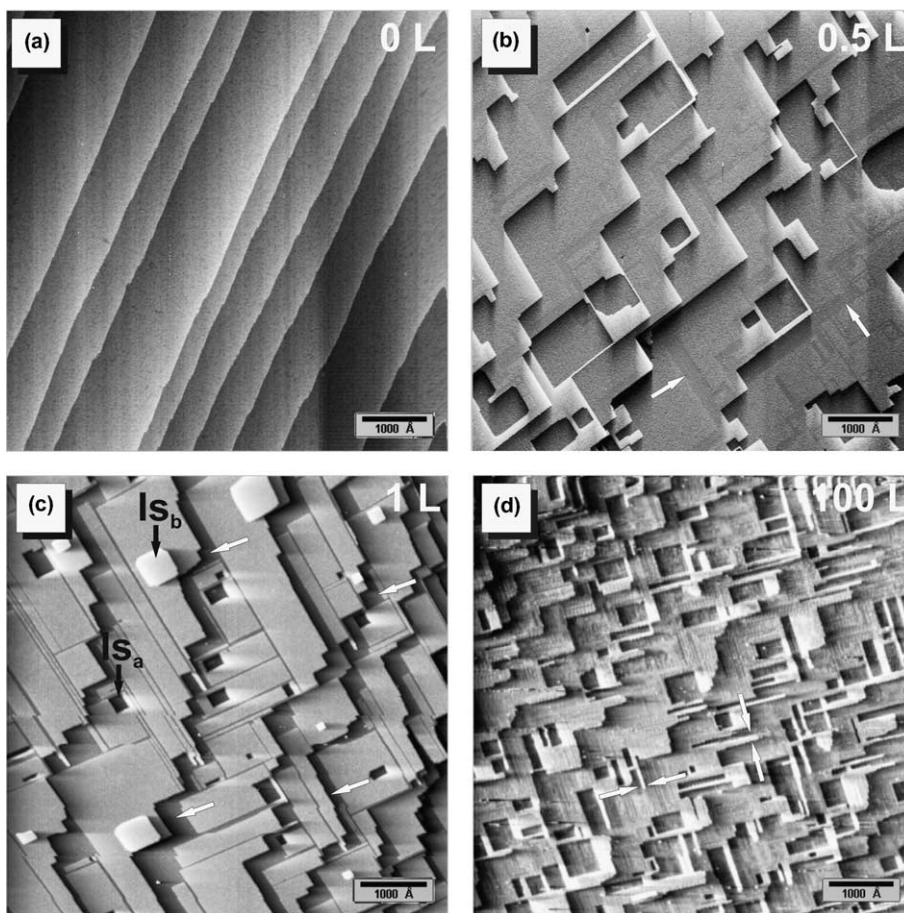


Fig. 6. Set of wide range STM images of CoAl(100) at different stages of oxidation. (a) Clean CoAl(100) surface ($U_t = 1.00$ V, $I_t = 0.2$ nA); (b) 0.5 L O₂ ($U_t = 2.04$ V, $I_t = 0.2$ nA); (c) 1 L O₂ ($U_t = 2.04$ V, $I_t = 0.2$ nA); (d) 100 L O₂ ($U_t = 0.154$ V, $I_t = 0.2$ nA).

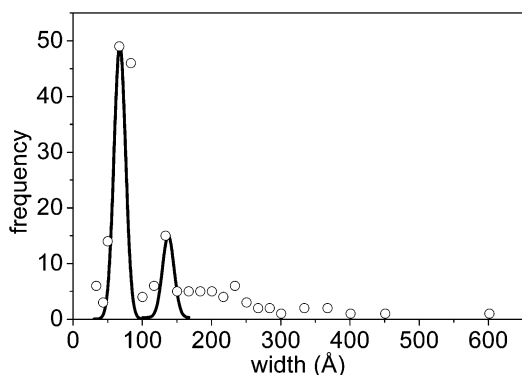


Fig. 7. The analysis of the stripes width distribution of Fig. 6d shows two pronounced maxima.

to the oxide film, caused by the lattice mismatch between θ -Al₂O₃ and CoAl(100), that prevents the lateral growth perpendicular to the streaks.

3.3. Temperature dependence of the oxidation of CoAl(100)

Now we focus on the temperature dependence of the growth of alumina on CoAl(100). We describe both the case of partially oxygen-covered CoAl(100) after the 1 L O₂ exposure and the case of an oxygen saturated surface (500 L O₂).

Fig. 8 shows the AES peak-to-peak ratios $I(\text{O}_{\text{KLL}}(503 \text{ eV}))/I(\text{Co}_{\text{LMM}}(775 \text{ eV}))$ as a function

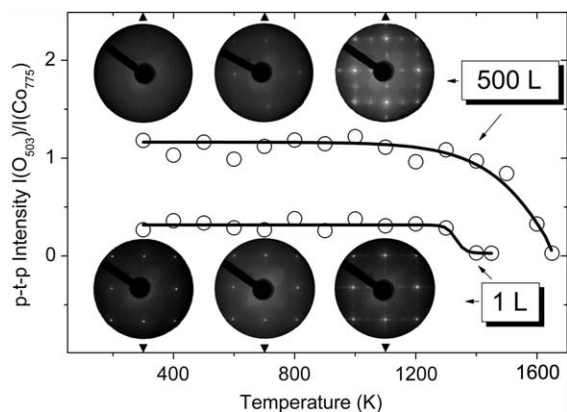


Fig. 8. Peak-to-peak intensity ratio of O_{KLL} (503 eV)/ Co_{LMM} (775 eV) as a function of annealing temperature for 1 and 500 L of O_2 on $CoAl(100)$. LEED pictures ($E_p = 75$ eV) of 500 L (top) and 1 L (bottom) oxygen on $CoAl(100)$ show structural changes during annealing.

of annealing temperature for the 1 L O_2 and 500 L O_2 exposures. After the exposure of 1 L O_2 the ratio amounts to 0.3 and remains constant up to annealing at 1300 K. After annealing at 1400 K the oxygen is fully desorbed. Although the constant ratio demonstrates that the amount of oxygen is constant LEED investigations reveal structural changes. After oxidation with 1 L of O_2 at 300 K the (1×1) patterns of the clean $CoAl(100)$ sample (Fig. 8 bottom) are still visible. While after the annealing at 700 K the LEED pattern do not change, additional weak spots and weak streaks along the $[100]$ and $[010]$ direction appear after annealing at 1100 K. The latter LEED patterns suggest formation of (2×1) structure with two perpendicularly aligned domains.

The peak-to-peak ratio of O and Co is 1.1 after the 500 L O_2 exposure at room temperature, showing that the oxidation is complete [6]. The ratio is constant up to 1300 K. Due to the oxide decomposition the ratio decreases for annealing temperatures above 1300 K and drops to zero at 1650 K. It should be mentioned that lower annealing temperatures are sufficient to remove the oxide, as well, at longer annealing time. For that reason, 1 L O_2 on $CoAl(100)$ was already desorbed after annealing at 1400 K. After oxidation at saturation level, the LEED screen exhibits only a diffuse illumina-

tion (Fig. 8 top). This indicates that the surface has lost long-range order and an $a-Al_2O_3$ film with a thickness of around 7 Å is grown [6]. After annealing at 700 K weak LEED spots at the $(\pm 1, 0)$ and $(0, \pm 1)$ positions can be found. Further annealing leads to an increase of the intensity of this spots. After 1000 K, again, a (2×1) LEED pattern can be obtained. The spot intensity increases with rising temperature. Finally, after 1650 K the (1×1) LEED pattern corresponding to the clean $CoAl(100)$ substrate appears (not shown).

The vibrational properties during the annealing have been investigated with EELS. Generally, we found that three regions exist with characteristic temperatures (300–500, 600–800 and 900–1300 K) and special vibrational properties. Fig. 9 presents typical EEL spectra from each range. After the 1 L O_2 exposure at 300 K the EEL spectrum exhibits losses at 370, 620 and 815 cm^{-1} (Fig. 9 left). It has been already presented in Ref. [6] that more than two modes can

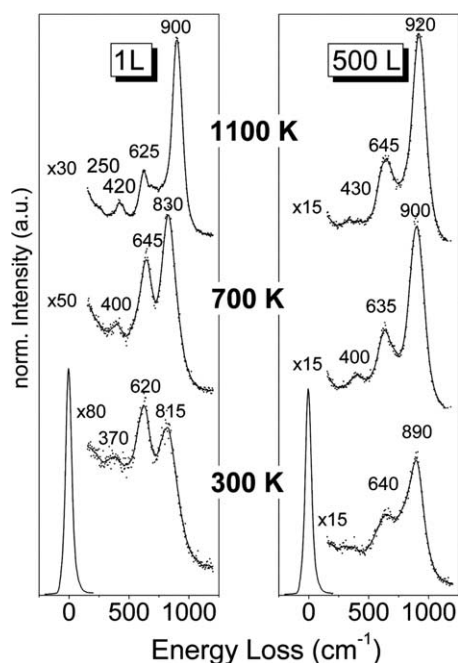


Fig. 9. EEL spectra of 1 L of O_2 (left) and 500 L of O_2 (right) for different annealing temperatures.

be expected for small oxygen exposures. A reasonable explanation is the existence of several different sites in which oxygen atoms are chemisorbed at low coverages. The ratio between the intense modes at 620 and 815 cm^{-1} amounts to 1.2. The ratio moves to lower values with increasing temperature. Annealing at 700 K inverts the ratio of the intensities. A different spectrum occurs with modes at 400, 645 and 830 cm^{-1} . This indicates a transition from $\alpha\text{-Al}_2\text{O}_3$ to a different oxide phase. In the thermal dehydration sequence of boehmite and of trihydroxides a phase transition to $\gamma\text{-Al}_2\text{O}_3$ occurs at about 700 K in vacuum [29]. The process involves an alteration of the occupation probability of tetrahedral and octahedral vacancies in the oxygen sub-lattice and may account for the change in the EEL spectrum. On the other hand, it is possible that in the temperature range between 600 and 800 K $\alpha\text{-Al}_2\text{O}_3$ transforms into disordered clusters of $\theta\text{-Al}_2\text{O}_3$. The absence of a (2×1) structure in LEED can be explained by both processes mentioned above. After annealing at 1100 K the EEL spectrum exhibits intense FK modes at 420, 625 and 900 cm^{-1} , characteristic for the temperature range between 800 and 1400 K. In agreement with the (2×1) spots in LEED, this spectrum can be assigned to well-ordered $\theta\text{-Al}_2\text{O}_3$. The weak shoulder at 250 cm^{-1} is the Al vibrational mode of the clean surfaces slightly shifted in energy. Generally, with increasing annealing temperature the intensity of the phonons in the EEL spectra gradually increase. Furthermore, the FWHM of the losses shrinks indicating a gain of ordering as a function of annealing temperature.

After a 500 L O_2 exposure at room temperature the EEL spectrum shows FK modes at 640 and 890 cm^{-1} (Fig. 9 right). These are the characteristic FK phonons of $\alpha\text{-Al}_2\text{O}_3$ [6]. After annealing at 700 K an additional loss appears at 400 cm^{-1} . The spectrum is characteristic for a well-ordered oxide, whereupon the formation of $\gamma\text{-Al}_2\text{O}_3$ is most likely. The EEL spectrum of the annealing at 1100 K exhibits modes at 430, 645 and 920 cm^{-1} and corresponds to the spectrum of $\theta\text{-Al}_2\text{O}_3$. A fourth mode, expected at around 780 cm^{-1} , is unresolved due to the broadness of the loss structure.

3.4. Band gap of $\theta\text{-Al}_2\text{O}_3/\text{CoAl}(100)$

Wide energy range EEL spectra were recorded to determine the band gap of well ordered alumina films on $\text{CoAl}(100)$. In order to gain intensity low energy resolution and long integration times were chosen. Fig. 10 shows spectra that cover a range of energy losses up to 10 eV. After the oxidation at 800 K the spectrum (Fig. 10a) exhibits intense FK modes in the low frequency region that were already observed in Fig. 3. In addition, a very broad loss structure around 4.5 eV appears, due to the excitations of electrons from the valence band into the conduction band of the oxide. Disregarding the matrix element effects, the loss probability is proportional to the joint density of states.

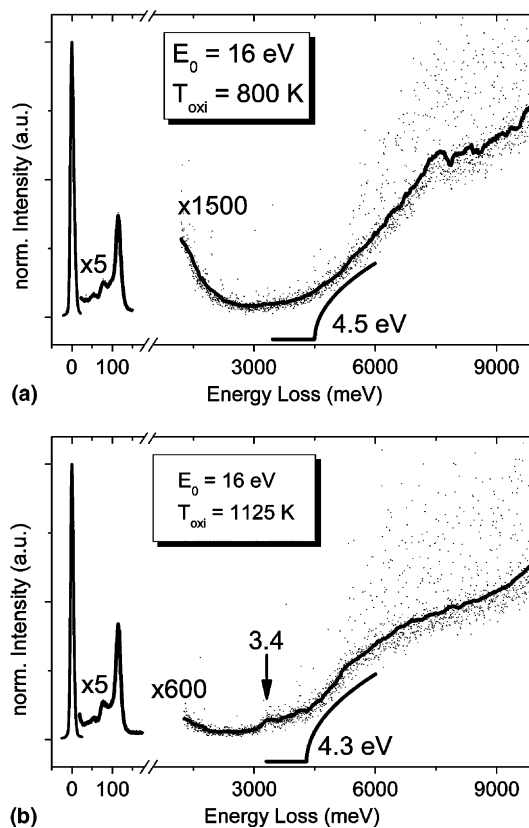


Fig. 10. Wide energy range EEL spectra of $\theta\text{-Al}_2\text{O}_3$ on $\text{CoAl}(100)$. The band gap of the film is indicated by the broad loss structure starting around (a) 4.5 eV after the growth at 800 K and (b) 4.3 eV at 1125 K accompanied by an isolated gap state at 3.4 eV.

Using a rough approximation with a parabolic shape of the maximum and minimum of the band edges the loss probability is proportional to $\Theta(\hbar\omega - E_g) \cdot (\hbar\omega - E_g)^{1/2}$, where Θ is the Heavy-side step function. The EEL spectrum was compared with this expression and yields a band gap of $E_g = 4.5$ eV. The band gap of $\alpha\text{-Al}_2\text{O}_3$ is ~ 3.2 eV [6]. This suggests that the well-ordered oxide film contains fewer defects. However, the band gap of bulk $\gamma\text{-Al}_2\text{O}_3$ is $E_g = 8.7$ eV [30]. Thus, the low band gap of well-ordered alumina on CoAl(100) may be due to defect-induced states in the band gap region.

An isolated gap state at 3.4 eV was observed after the oxidation of CoAl(100) at 1125 K (Fig. 10b). It may be related to surface states or may originate from interface states of the insulating oxide film and the CoAl substrate, e.g. metal-induced gap states. Also the existence of deep impurities or defect levels can be responsible for this feature. However, the spectrum yields a band gap of 4.3 eV showing the electrical similarity of the oxide films prepared at high temperatures.

4. Summary

In conclusion, we have used AES, EELS, LEED and STM to investigate the growth of Al_2O_3 on CoAl(100) at elevated temperatures. Oxidation at 800 K leads to the growth of well-ordered $\theta\text{-Al}_2\text{O}_3$ with a self-limiting thickness with saturation at 9–10 Å. We found that this oxide films has a band gap ~ 4.5 eV. The $\theta\text{-Al}_2\text{O}_3$ grows in two domains perpendicular to each other. After oxygen saturation, the surface shows typical oxide stripes supposedly related to the mismatch between the substrate and the oxide. Oxidation at room temperature with subsequently annealing leads to a phase transition from amorphous to well-ordered oxide. A thermal stability of the oxide film up to around 1400 K was found.

Acknowledgment

This work is dedicated to our friend and colleague Prof. René Franchy who passed away on May 8, 2004.

References

- [1] P.L.J. Gunter, J.W.H. Niemantsverdriet, F.H. Ribeiro, G.A. Somorjai, Catal. Rev. Sci. Eng. 39 (1997) 77.
- [2] E. Hirota, H. Sakakima, K. Inomata, Giant Magneto-Resistance Devices, Springer, Berlin, 2002.
- [3] R. Franchy, Surf. Sci. Rep. 38 (2000) 195.
- [4] H. Graupner, L. Hammer, K. Heinz, D.M. Zehner, Surf. Sci. 380 (1997) 335.
- [5] M. Cooper, Phil. Mag. 89 (1963) 805.
- [6] V. Rose, V. Podgursky, I. Costina, R. Franchy, Surf. Sci. 541 (2003) 128.
- [7] V. Blum, L. Hammer, Ch. Schmidt, W. Meier, O. Wieckhorst, S. Müller, K. Heinz, Phys. Rev. Lett. 89 (2002) 266102.
- [8] H. Ibach, Electron Energy Loss Spectrometer, The Technology of High Performance Springer Series in Optical Science, vol. 63, Springer, Berlin, 1991.
- [9] K. Besocke, Surf. Sci. 181 (1987) 145.
- [10] D.R. Lide (Ed.), Handbook of Chemistry and Physics, 75th ed., CRC, London, 1996.
- [11] N. Cabrera, N.F. Mott, Rep. Prog. Phys. 12 (1948–1949) 163.
- [12] Tanuma, C.J. Powell, D.R. Penn, Surf. Interf. Anal. 17 (1991) 927.
- [13] S.C. Lui, J. Mundenar, E.W. Plummer, M.E. Mostoller, R.M. Nicklow, D.M. Zehner, W.K. Ford, J. Erskine, in: D.M. Zehner, D.W. Goodman (Eds.), Physical and Chemical Properties of Thin Metal Overlayers and Alloy Surfaces, Mater. Res. Soc. Symp. Proc., vol. 83, MRS, Pittsburgh, 1987, p. 47.
- [14] K. Kitamura, T. Nagao, T. Osaka, R. Franchy, C. Oshima, Jpn. J. Appl. Phys. 32 (1993) 3252.
- [15] K.L. Kliewer, R. Fuchs, Phys. Rev. 144 (1966) 495.
- [16] R. Fuchs, K.L. Kliewer, Phys. Rev. 140 (1965) A2076.
- [17] Gassmann, R. Franchy, H. Ibach, Surf. Sci. 319 (1994) 95.
- [18] M. Jaeger, K. Kuhlenbeck, H.-J. Freund, M. Wuttig, W. Hoffmann, R. Franchy, H. Ibach, Surf. Sci. 259 (1991) 235.
- [19] R. Franchy, J. Masuch, P. Gassmann, Appl. Surf. Sci. 93 (1996) 317.
- [20] I. Costina, R. Franchy, Appl. Phys. Lett. 78 (2001) 4139.
- [21] C. Becker, J. Kandler, R. Raaf, R. Linke, T. Pelster, M. Dräger, M. Tanemura, K. Wandelt, J. Vac. Sci. Technol. A 16 (1998) 1000.
- [22] R.L. Strong, B. Firey, F.W. de Wette, J.L. Erskine, Phys. Rev. B 26 (1982) 3483.
- [23] Ph. Lambin, J.-P. Vigneron, A.A. Lucas, Comp. Phys. Comm. 60 (1990) 351.
- [24] J.J. Rechten, C.R. Kannewurf, J.O. Brittain, J. Appl. Phys. 38 (1967) 3045.
- [25] Y.T. Chu, J.B. Bates, C.W. White, G.C. Farlow, J. Appl. Phys. 64 (1988) 3727.
- [26] R.-P. Blum, D. Ahlbehrendt, H. Niehus, Surf. Sci. 396 (1998) 176.

- [27] A. Stierle, V. Formoso, F. Comin, R. Franchy, *Surf. Sci.* 467 (2000) 85.
- [28] R. Franchy, M. Eumann, G. Schmitz, *Surf. Sci.* 470 (2001) 337.
- [29] B.G. Linsen (Ed.), *Physical and Chemical Aspects of Adsorbents and Catalysts*, Academic Press, London, 1970.
- [30] F.S. Ohuchi, R.E. French, *J. Vac. Sci. Technol. A* 6 (1987) 1695.